European Journal of Pharmaceutics and Biopharmaceutics 142 (2019) 20–30

Contents lists available at ScienceDirect

European Journal of Pharmaceutics and Biopharmaceutics

journal homepage: www.elsevier.com/locate/ejpb

Research paper

Ocular biocompatibility of dexamethasone acetate loaded poly(ε-caprolactone) nanofibers

Gisele Rodrigues Da Silva[a], Tadeu Henrique Lima[b], Gabriella Maria Fernandes-Cunha[c], Rodrigo Lambert Oréfice[b], Armando Da Silva-Cunha[c], Min Zhao[d,e], Francine Behar-Cohen[d,e,f,*]

[a] School of Pharmacy, Federal University of Ouro Preto, Ouro Preto, Minas Gerais 35400-000, Brazil
[b] Department of Metallurgical and Materials Engineering, Federal University of Minas Gerais, Belo Horizonte, Minas Gerais 31270-901, Brazil
[c] School of Pharmacy, Federal University of Minas Gerais, Belo Horizonte, Minas Gerais 31270-901, Brazil
[d] Centre de recherche des Cordeliers, Inserm UMR1138, Paris, France
[e] Université René Descartes Sorbonne Paris Cité, Paris 75006, France
[f] Ophthalmopole, Hôpital Cochin, Assistance Publique Hôpitaux de Paris, France

ARTICLE INFO

Keywords:
Electrospinning technique
Electrospun nanofibers
Nanofibers
Poly(ε-caprolactone)
Dexamethasone acetate
Dexamethasone acetate-loaded poly(ε-caprolactone) nanofibers

ABSTRACT

Electrospinning technique has been explored to produce nanofibers incorporated with drugs as alternative drug delivery systems for therapeutic purposes in various organs and tissues. Before such systems could potentially be used, their biocompatibility must be evaluated. In this study, dexamethasone acetate-loaded poly(ε-caprolactone) nanofibers (DX PCL nanofibers) were developed for targeted delivery in the vitreous cavity in the treatment of retinal diseases. Ocular biocompatibility was tested *in vitro* and *in vivo*. DX PCL nanofibers were characterized by scanning electron microscopy (SEM) and Fourier Transform InfraRed spectroscopy (FTIR) and the *in vitro* drug release from nanofibers was evaluated. The *in vitro* biocompatibility of DX PCL nanofibers was tested on both ARPE-19 and MIO-M1 cells using the cytotoxicity (MTT) test by morphological studies based on staining of the actin fibers in ARPE-19 cells and GFAP in MIO-M1 cells. The *in vivo* biocompatibility of DX PCL nanofibers was investigated after intravitreous injection in the rat eye, using spectral domain Optical Coherence Tomography (OCT) imaging of the retina. SEM results indicated that nanometric fibers were interconnected in a complex network, and that they were composed of polymer. FTIR showed that polymer and drug did not chemically interact after the application of the electrospinning technique. PCL nanofibers provided controlled DX release for 10 days. DX PCL nanofibers were not cytotoxic to the ocular cells, allowing for the preservation of actin fibers and GFAP in the cytoplasm of ARPE-19 and MIO-M1 cells, respectively, which are biomarkers of these ocular cell populations. DX PCL nanofibers did not affect the retinal and choroidal structures, and they did not induce abnormalities, hemorrhages, or retinal detachment, suggesting that the nanofibers were well tolerated. In eyes receiving DX PCL nanofibers, SD-OCT images were corroborated with histological analysis of neuroretina and choroid, which are ocular tissues that are extremely sensitive to toxic agents. Finally, the preservation of cone and rod photoreceptors indicated the light sensitivity of the animals. In conclusion, DX PCL nanofibers exhibited ocular biocompatibility and safety in the rodent eye and allow the release of dexamethasone. Further studies are required to appreciate the potential of these new drug delivery systems for the treatment of retinal diseases.

1. Introduction

The electrospinning technique allows the formation of ultrafine fibers with micro to nanometer range diameters. In the electrospinning method, drops of the polymer solution are submitted to a strong electric field and are formed into conical objects. When the voltage surpasses a threshold value, the electric force overcomes the surface tension of the droplet, and one or multiple charged jets of the solution are ejected from the tip of the droplet. As the jet moves toward a collecting metal screen (counter electrode), the solvent evaporates and a non-woven fabric mat is formed on the screen [1,2,3]. Nanofiber mats with loaded drug and/or bioactive substances can be prepared by applying

* Corresponding author.
E-mail addresses: giselersilva@ufop.edu.br (G.R. Da Silva), rorefice@demet.ufmg.br (R.L. Oréfice), armando@farmacia.ufmg.br (A. Da Silva-Cunha), francine.behar@parisdescartes.fr (F. Behar-Cohen).

https://doi.org/10.1016/j.ejpb.2019.05.010
Received 21 December 2018; Received in revised form 21 March 2019; Accepted 10 May 2019
Available online 24 May 2019

electrospinning process.

Electrospun polymer nanofibers showed excellent biocompatibility, biodegradability, high porosity, and controllable mechanical properties [4]. Moreover, ultrafine fibers exhibit distinctive features compared to the bulk material due to their small dimensions and large surface-area-to-volume ratio [5]. Considering the attractive characteristics of polymeric nanofibers, these biomaterials have been explored as natural extracellular matrix in tissue engineering, since they are capable of supporting the adhesion, proliferation and differentiation of cells, preserving cell morphology. In addition, their porosity allows cell migration and the efflux of nutrients and metabolic products produced by those cells [6]. In ocular tissue engineering, nanofibrous substrates were proposed to support the adhesion and growth of human retinal pigment epithelium (RPE) cells for subretinal transplantation [7], and for future cell-based therapy in blinding retinal diseases [8].

Nanofibers have also been investigated as controlled drug delivery systems deployed for the treatment of local pathologies. Nanofibers present the advantages of providing high drug loading capacity, high drug encapsulation efficiency and simultaneous delivery of diverse therapeutic agents [1]. Furthermore, fibers can help the drug cross physiological barriers, decrease premature drug release, and target tissues while minimizing drug distribution elsewhere in the body [9]. Nanofibers provide controlled drug release over prolonged periods, which is essential in treating chronic diseases. Considering their applicability as drug carriers in the ophthalmological area, polymeric nanofibers were incorporated into timolol maleate, which coated the exterior of contact lenses to reduce intraocular pressure and, consequently, to treat glaucoma [10]. Nanofibers loaded with triamcinolone acetonide, an anti-inflammatory drug reduced inflammation in rat experimental autoimmune uveitis [11]. In addition, electrospun nanofibers based on chitosan and triamcinolone acetonide provided the controlled and prolonged release of the drug following the zero-order kinetic profile [12]. Nanofiber scaffolds incorporated into peptide amphiphile molecules carrying bioactive peptide sequences derived from laminin and fibronectin were released to induce corneal stroma regeneration [13]. Finally, biodegradable core shell nanofibers composed of bevacizumab, an antiangiogenic antibody that neutralizes VEGF, were designed to inhibit choroidal neovascularization associated with age-related macular degeneration [14].

In this study, nanofibers made of poly(ε-caprolactone) and dexamethasone acetate were developed to deliver corticosteroids to the back of the eye during the post-operative period of any vitreoretinal disease. Poly(ε-caprolactone) was selected to compose the nanofibers since we previously described that nanostructured scaffolds based on this polymer did not elicit inflammatory and immune responses or toxicity after their implantation in the vitreous cavity of rat's eyes, demonstrating their intraocular biocompatibility [15]. As the ocular compatibility was achieved by poly(ε-caprolactone) in a nanoscale organization, these nanofibers were incorporated into dexamethasone acetate due to its high anti-inflammatory potency and its extensive use in the treatment of ocular inflammatory diseases. In addition to its anti-inflammatory action, this steroid is also an immunosuppressive and anti-angiogenic drug [16]. The nanofibers composed of poly(ε-caprolactone) and dexamethasone acetate were characterized by scanning electron microscopy (SEM) to verify the morphology of nanostructure fibers and by Fourier transform InfraRed spectroscopy (FTIR) to investigate possible chemical interactions between the components. The mass loss of polymeric nanofibers and the *in vitro* dexamethasone acetate release were evaluated. Finally, considering the importance of evaluating the ocular biocompatibility of these nanofibers, the response of Muller glial cells (MIO-M1) and retinal pigment epithelial cells (ARPE-19) to direct contact with the dexamethasone acetate-loaded nanofibers, the released drug, and the polymeric by-products was determined in terms of viability and capability to proliferate and differentiate. These two types of human ocular cells were chosen because they have been shown to be sensitive to glucocorticoids, undergoing cell death at dexamethasone threshold concentrations [17]. Furthermore, nanofibers were inserted into the vitreous cavity of rat eyes to investigate their tolerance *in vivo*, which was determined by retinal imaging, histology and staining of cone photoreceptors.

To date, the treatment of post-operative inflammation following vitreoretinal surgery is based on repeated local and eventually systemic administration of anti-inflammatory drugs. However, systemic side effects are limiting and topical treatments are associated with poor compliance. Whilst intraocular biodegradable or non-biodegradable solid implants corticosteroids for several months are adapted to treat chronic intraocular inflammation [18], there are no drug delivery systems allowing the release of anti-inflammatory agents for the post-operative period. Intraocular nanofibers composed of poly(ε-caprolactone) and dexamethasone acetate could represent a potential alternative therapy for this indication.

2. Materials and methods

2.1. Preparation of nanofibers

Poly(ε-caprolactone) (PCL, MW ~80,000–90,000 g/mol; Sigma Chemical Co., USA) solution [14.6% (w/v)] was prepared by dissolving PCL pellets in a mixture of acetic acid and formic acid (1:1) (Sigma Aldrich, St. Louis, MO) under magnetic stirring for 3 h at room temperature. Dexamethasone acetate (DX, Sigma Chemical Co., USA) solution [20% (w/v)] was prepared by dissolving DX in a mixture of acetic acid and formic acid (1:1). Clear solutions were electrospun using an electrospinning setup consisting of a dual polarity, high-voltage DC power supply unit (Gamma High Voltage Research, Ormond Beach, FL), a syringe pump (Arti Glass, CE, Italy), syringe (Arti Glass, CE, Italy), and a needle (22 G) with blunted tip. The positive terminal of the high-voltage supply was connected to the needle tip while the negative terminal was connected to a metallic collector plate; a voltage of +25 kV was maintained between them. Electrospun fibers were collected on coverslips held over the metallic collector disc (8 cm diameter). Flow rate was maintained at 3.6 mL/h and needle tip to collector distance was maintained at 9 cm. DX-loaded PCL nanofibers (DX PCL nanofibers), as well as blank nanofibers (PCL nanofibers), were prepared.

2.2. Characterization

2.2.1. Morphology and diameter of nanofibers

The morphology and diameter of nanofibers were analyzed by scanning electron microscopy (SEM) (JEOL JSM 5600, Japan) at an accelerating voltage of 15 kV. Samples for SEM were mounted on metal stubs and coated with gold using a sputter coater (JEOL JFC-1200 fine coater, Japan). Nonwoven nanofiber mats were analyzed with 50 individual measurements of nanofiber diameters taken from SEM micrographs using image analysis software (ImageJ, National Institutes of Health, USA). This was repeated for a single electrospun fiber mat fabricated under a single set of constant conditions to calculate the average nanofiber diameter and standard deviation [15].

2.2.2. Determination of DX incorporated into the PCL nanofibers

For the determination of content uniformity of DX incorporated into the nanofibers, the following procedure was performed: one mat was cut into disks of 4.5 mm diameter. Ten spheres (DX PCL nanofibers) were selected and weighed. Each nanofiber sphere was dissolved in 3 mL of acetonitrile, and the volume of the volumetric flask (5 mL) was completed with ultrapure water. Solutions were filtered through a 0.22 μm filter. The amount of DX present in each nanofiber sample was determined by a high performance liquid chromatographic (HPLC) method described for this drug in The United States Pharmacopeia [19]. The standard solution of DX was also prepared as described above. The uniformity content of DX in the nanofibers was expressed as the percent

of the pre-indicated value (approximately 200 μg). The relative standard deviation was also calculated.

2.2.3. Fourier transform InfraRed spectroscopy (FTIR)

Infrared spectra were collected in a FTIR spectrophotometer (Perkin Elmer, model Spectrum 1000). Measurements were carried out using the attenuated total reflectance (ATR) technique. Each spectrum was a result of 32 scans with a resolution of 4 cm^{-1}.

2.2.4. Measurement of mass loss of PCL nanofibers

In vitro degradation study was performed by recording the mass loss of PCL nanofibers over 12 days in phosphate-buffered saline (PBS, pH 7.4). Nanofibers (spheres of 4.5 mm diameter) were placed in different tubes containing 300 μL of PBS (n = 6). These tubes were placed inside an incubator set at 37 °C and 30 rpm. At each time point (0, 1, 2, 4, 6, 8, 10 and 12 days), nanofibers were retrieved from the PBS, rinsed with deionized water, and vacuum-dried for 48 h before mass loss was analyzed. The cumulative percentage of mass loss was calculated and the results were plotted in a graph.

2.3. In vitro release profile

Five nanofibers (spheres of 4.5 mm diameter) were immersed inside different tubes containing 36.6 mL of PBS. Tubes were placed inside a shaker incubator set at 37 °C and 30 rpm. At predetermined intervals (0, 1, 2, 4, 6, 8, 10 and 12 days), 36.6 mL of the medium was sampled and 36.6 mL of fresh medium was immediately added to each tube. The medium was freeze-dried. The amount of DX released was measured using the HPLC method described in The United States Pharmacopeia [19].

2.4. In vitro biocompatibility study

2.4.1. ARPE-19 and Müller glial cell (MIO-M1 cell) cultures

ARPE-19 cells, an established spontaneously arising human RPE cell line, were grown in Dulbecco's Modified Eagle's Medium and Ham's F12 medium (DMEM/F12 Gibco BRL:Grand Island, NY) with 10% fetal bovine serum (FBS Gibco BRL: Grand Island, NY) in a 37 °C humidified atmosphere of 5% CO_2 and 95% air [15]. Müller glial cells (MIO-M1 cells), a spontaneously immortalized RMG cell line that originated from human retina [20], were grown in Dulbecco's Modified Eagle's Medium/Glutamax (DMEM/Glutamax Gibco BRL:Grand Island, NY) with 10% fetal bovine serum (FBS Gibco BRL:Grand Island, NY), 0.4% gentamicin, and 0.1% amphotericin B at 37 °C in a humidified atmosphere of 5% CO_2 and 95% air. The culture medium of both cell populations was refreshed every 2 days. Upon confluence, cells were rinsed with 2 mL of a 0.05% trypsin-EDTA (Gibco, Grand Island, NY) solution and incubated with 5 mL of trypsin-EDTA at 37 °C in a humidified atmosphere of 5% CO_2 and 95% air. Next, within 5–15 min, the trypsin enzyme activity was halted by the addition of 5 mL of complete growth medium and the cells were centrifuged for 5 min at 1500 rpm. The supernatant was discarded, while the cells were resuspended in 13 mL of fresh medium and seeded onto culture flasks for further propagation and subsequent passages [15].

2.4.2. ARPE-19 and MIO-M1 cell cultures in contact with nanofibers

Nanofibers were cut into round pieces (4.5 mm in diameter) and exposed to UV light for 90 min on each side prior to cell culture. ARPE-19 and MIO-M1 cells were plated in contact with the nanofibers and control tissue culture polystyrene (TCPS) (Costar, Cambridge, MA) at a density of 4×10^3 cells/well [15].

2.4.3. ARPE-19 and MIO-M1 cell proliferation in contact with nanofibers (nuclear count)

After 1, 2, 5 and 10 days in culture, the medium was aspirated, and ARPE-19 and MIO-M1 cells in contact with nanofibers and control TCPS were rinsed once with PBS and then fixed in *para*-formaldehyde 4% (v/v) (Merck Eurolab, Fontelay Sous-Bois, France) for 15 min. Next, the fixed cells were rinsed again with PBS for 5 min and then immersed in PBS containing 0.3% (v/v) Triton X-100 (Sigma-Aldrich) for 15 min. After rising in PBS for 5 min, nuclei were stained with 4,6-diamidino-2-phenylindole (DAPI) (Sigma-Aldrich) in PBS (1:1250) for 5 min at room temperature. Finally, cells were washed five times at 5 min intervals with PBS and one time with water, mounted in Gel Mount (Biomeda, Burlingame, CA), and viewed using an Olympus IX70 fluorescence microscope attached to a digital camera (Olympus DP70). Five fields were photographed per nanofiber and control TCPS (total of 15 fields per surface per timepoint). Nuclei were counted for each field of view (0.59 mm^2). The average number of nuclei on the control surface was set as 100%, while the average number of nuclei ± standard deviation in contact with the nanofibers was obtained as a percentage of the control as previously described [15].

2.4.4. Cytotoxicity of nanofibers

After 1, 2, 5 and 10 days in the culture, the medium was aspirated, and ARPE-19 and MIO-M1 cells in contact with the nanofibers and control TCPS were rinsed with PBS. ARPE-19 and MIO-M1 cells were incubated with 150 μL of 3-[4,5-dimethylthiazol-2-yl]-2,5-diphenyltetrazolium bromide (MTT) (1 mg/mL in PBS) (Sigma Chemical, Saint Louis, CO). After 3 h of incubation, cells were lysed with 100 μL of isopropanol, and absorbance values were measured at 570 nm versus 630 nm using a microplate reader (BioRad, San Diego, CA). The mean absorbance on the control surface was set as 100%, while the mean absorbance ± standard deviation in contact with the nanofibers was obtained as a percentage of the control as previously described [15].

2.4.5. Morphology of ARPE-19 and MIO-M1 cells – Immunofluorescence

After 10 days of culture, ARPE-19 and MIO-M1 cells in contact with the nanofibers and control TCPS were subjected to the same procedure described for the proliferation study. After nuclear staining with DAPI, F-actin fibers were labeled with Phalloidin FITC (Sigma-Aldrich) in PBS (1:250) for 30 min at room temperature. Cells were rinsed, mounted, and viewed using an Olympus IX70 fluorescence microscope attached to a digital camera (Olympus DP70). At 10 days of culture, for the labeling of glial fibrillary acidic protein (GFAP), the MIO-M1 cells grown in contact with the nanofibers and control TCPS were fixed with *para*-formaldehyde 4% (v/v) for 30 min at room temperature. Fixed cells were incubated with PBS containing Triton X-100 0.1% (v/v) for 30 min. This was followed by incubation with polyclonal rabbit antibody against GFAP (1:100) (Dako, Trappes, France) at room temperature for 3 h. After washing with PBS, an Alexa Fluor 488-conjugated goat anti-rabbit IgG (1:100) (Molecular Probes, Leiden, The Netherlands) was applied for 60 min in the dark. Finally, nuclei were stained with DAPI (Sigma-Aldrich) in PBS (1:1250) for 5 min at room temperature. Then, cells were rinsed five times, mounted, and viewed using an Olympus IX70 fluorescence microscope attached to a digital camera (Olympus DP70) [15].

2.5. In vivo biocompatibility study

2.5.1. Animals

Female Lewis rats (8–12 weeks old; Janvier, Le Genest-Saint-Isle, France) were kept in pathogen-free conditions with food and water *ad libitum* and housed in a 12-h light/12-h dark cycle. Animals were divided into two groups: (1) rats without nanofibers (control group); and (2) rats receiving DX PCL nanofibers into the vitreous cavity. For each experimental series, the number of animals was indicated in the figure legends. All experiments were performed in accordance with the European Community's Council Directive 86/609/EEC and approved by ethical committees of Université René Descartes.

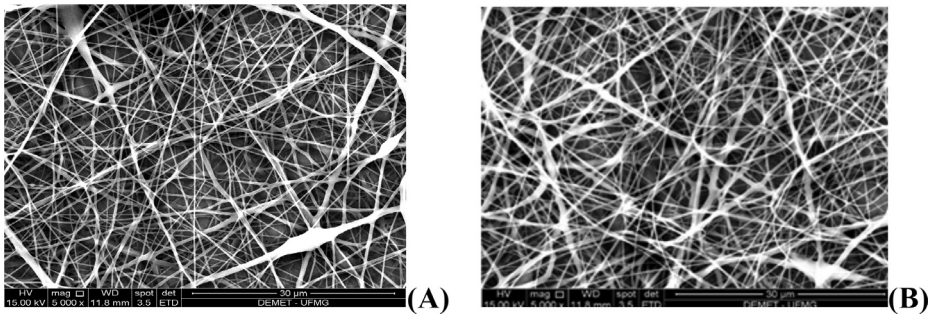

Fig. 1. SEM photomicrograph of PCL nanofibers (A) and DX PCL nanofibers (B). Magnification − 5000 × . Scale bar – 30 μm.

2.5.2. Implantation of DX PCL nanofibers into the vitreous cavity

Nanofibers of 1 mm were sterilized as previously described. Animals were anaesthetized with an intraperitoneal injection of xylazine (20 mg/kg) and ketamine (80 mg/kg). The left pupil was dilated with 0.5% (w/v) tropicamide eye drops (Théa Pharma, France). To implant the DX PCL nanofibers into the vitreous cavity, the conjunctiva was dissected at the limbus in the temporal superior quadrant, and a 1 mm sclerotomy was performed 2 mm posterior to the limbus. DX PCL nanofibers were introduced into the vitreous cavity through a transscleral injection [15].

2.5.3. Spectral domain optical coherence tomography (SD-OCT)

In vivo assessment of rat choroids and retinas was performed on anesthetized animals using spectral domain optical coherence tomography (SD-OCT; Spectralis device) adapted for small animal eyes [21]. Pupils were dilated with 0.5% (w/v) tropicamide drops (Théa pharma, France). Scans were acquired 10 days after the implantation of DX PCL nanofibers into the vitreous cavity of rat eyes. Rats of the control group were subjected to the same OCT evaluation. Temporal, nasal, and superior quadrants of retina were analyzed using the optic nerve head and the retina vessels as landmarks. Each 2-dimensional B-scan recorded at 30° field of view consisted of 1,536 A-scans with an optical resolution reaching 3.5 μm, and the enhanced depth imaging option was used to evaluate the choroid and retina. Retinal layers and choroid thickness were measured manually every 100 μm from the peripheral to the posterior pole. For analysis, retina and choroid were divided into 3 zones: periphery, middle, and posterior pole. In the middle section, 3–4 individual measurements were performed per rat (n = 5 per group).

2.5.4. Morphology

Animals of both groups were sacrificed using a lethal dose of pentobarbital (100 mg/kg – intraperitoneal injection) at 10 days of the experiment. Enucleated eyes were fixed in glutaraldehyde 2.5% (v/v) in cacodylate buffer (0.1 mol/L, pH 7.4). After 5 h of fixation, the eyes were dehydrated in a graded alcohol series (50%, 70%, 95%, and 100%) and embedded in epoxy resin. Semi-thin sections (1 μm) were cut using an ultramicrotome (Reichert Ultracut E, Leica, Wetzlar, Germany) and stained with toluidine blue. The morphology was examined under a light microscope (Olympus IX70) attached to a digital camera. Retinal layers and choroid thickness were measured manually every 100 μm from the peripheral to the posterior pole. For analysis, retinas and choroids were divided into 3 zones: periphery, middle, and posterior pole. In the middle section, 3–4 individual measurements were performed per rat (n = 3 per group).

2.5.5. Immunohistochemistry on cryosections

Animals of both groups were sacrificed using a lethal dose of pentobarbital (100 mg/kg – intraperitoneal injection) at 10 days of the experiment. Enucleated eyes were used for cryosections. Cryostat sections were incubated with primary antibodies: rabbit anti-cone arrestin (1:100; Millipore) and mouse anti-rhodopsin (Rho4D2, 1:100; Abcam), and secondary antibodies: FITC-conjugated peanut agglutinin (PNA, 1:100; Sigma-Aldrich) and Alexa Fluor 488-conjugated goat anti-mouse IgG (1:200; Invitrogen). Cell nuclei were stained with DAPI (1:3000; Sigma-Aldrich). Images were obtained using a fluorescence microscope (BX51; Olympus) [4].

2.6. Statistical analysis

Results were expressed as the mean ± standard deviation. Data were tested for normality and investigated for statistical significance using Student's *t*-test and one-way analysis of variance (ANOVA), where appropriate. A p-value below 0.05 was considered as significant.

3. Results

3.1. Characterization

3.1.1. Morphology and diameter of nanofibers

Fig. 1 shows PCL nanofibers (Fig. 1A) and DX PCL nanofibers (Fig. 1B) were successfully produced by electrospinning. SEM images of the nanofibers revealed the interconnectivity and random orientation of the fibers. The three-dimensional network showed high porosity. The average fiber diameters were 129 ± 22 nm and 145 ± 17 nm for PCL nanofibers and DX PCL nanofibers, respectively. Measurements indicated that the incorporation of DX tended to induce a slight increase in fiber diameter.

3.1.2. Determination of the content of DX incorporated into the PCL nanofibers

PCL mats containing the DX were cut into spheres of 4.5 ± 0.6 mm of diameter. The DX content within the PCL nanofibers (spheres) was 200.00 ± 0.04 μg and the standard deviation was 1.46%, which indicated that the drug was uniformly distributed into the nanometric fibers as required by the United States Pharmacopoeia [18].

3.1.3. Fourier transform InfraRed spectroscopy (FTIR)

Fig. 2 shows the FTIR spectra of PCL nanofibers (Fig. 2A) and DX PCL nanofibers (Fig. 2B). The InfraRed spectrum of blank nanofibers showed typical bands of the polymer, including bands at 1170 cm^{-1} and at 1240 cm^{-1}, corresponding to symmetric and asymmetric COC stretching vibrations, respectively; a band at 1293 cm^{-1}, indicating the C—C and C—O stretching modes in the crystalline PCL [22]; a band at 1722 cm^{-1}, related to the C═O stretching vibration; and finally bands at 2865 cm^{-1} and 2945 cm^{-1}, corresponding to the symmetric and asymmetric CH_2 stretching vibrations, respectively. FTIR results obtained from PCL nanofibers were similar to those previously described [23]. The InfraRed spectrum of DX PCL nanofibers revealed that the bands attributed to the polymer were entirely presented. However, the bands at 2865 cm^{-1} and 2945 cm^{-1}, corresponding to the CH_2 stretching vibrations from the polymer, were more intense in this FTIR spectrum than the same bands in the FTIR spectrum of blank nanofibers due to the overlapping of the band correspondent to the CH_2 stretching vibration from the DX molecule. The band at 1722 cm^{-1}, related to the

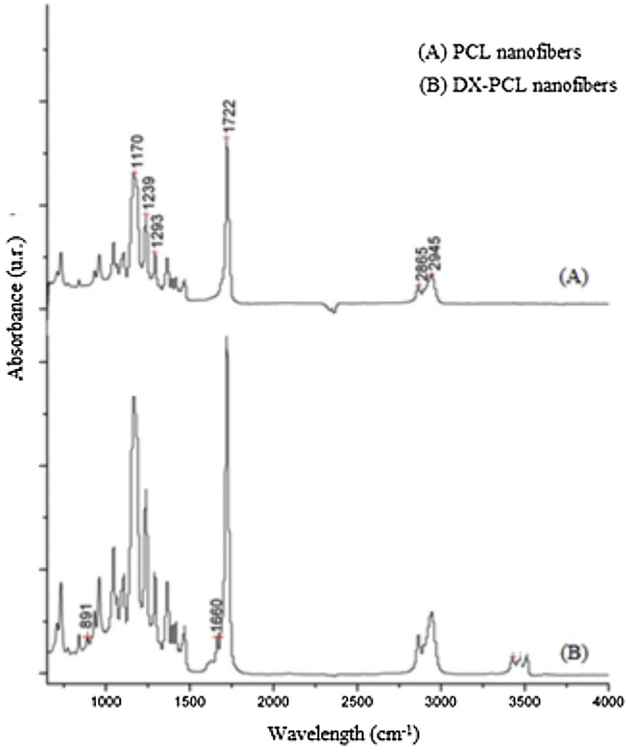

Fig. 2. FTIR spectra of PCL nanofibers (A) and DX PCL nanofibers (B).

C═O stretching vibration from the polymer, was also more intense and broadened due to two probable reasons: (1) the superposition of the band attributed to the C═O stretching vibration of ester groups from the DX structure; and (2) the hydrolysis of the ester bonds in PCL chains led to the formation of carboxyl groups. This hydrolysis occurred during solution preparation, in the presence of organic acids, and during electrospinning. Aband at approximately 3500 cm^{-1} was identified in this spectrum, which was attributed to the presence of −OH groups derived from the hydrolysis of the ester bonds of PCL [23,24]. Bands at 1660 cm^{-1} and 891 cm^{-1} were also detected, which were associated with the C═O stretching vibrations of aliphatic ketone groups and C-F axial deformation from the drug molecule, respectively.

3.1.4. Measurement of mass loss of PCL nanofibers

Fig. 3 represents the *in vitro* degradation of PCL nanofibers. The mass loss of the polymer was progressive, and only approximately 5% of the initial mass of nanofibers remained after the period of 12 days of immersion in PBS (pH 7.4). The water penetrated into the polymeric chains and induced the hydrolysis of the ester bonds present in PCL

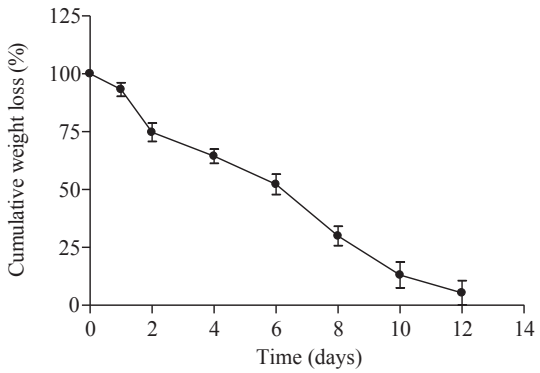

Fig. 3. Evolution of the mass loss of PCL nanofibers over a 12 days period. The results represent mean ± standard deviation (n = 5).

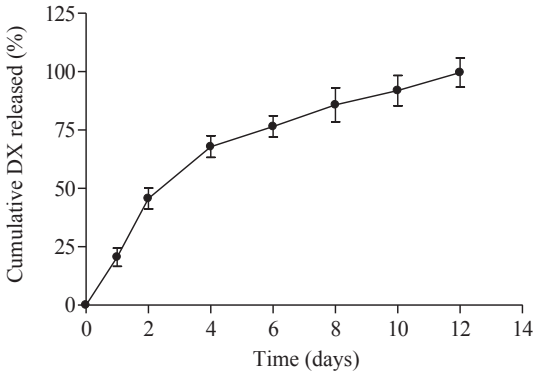

Fig. 4. *In vitro* release profile of DX from PCL nanofibers over a 12 day period. The results represent mean ± standard deviation (n = 5).

segments [25]. This hydrolytic process led to the mass loss of the polymer.

3.2. In vitro release profile

Fig. 4 depicts the *in vitro* release profile of DX from PCL nanofibers. During the first 2 days, approximately 47% of DX was released from the nanostructured polymer, which represented a burst release. From 2 to 12 days, the drug release from PCL nanofibers was controlled and sustained, and almost 100% of DX was delivered.

3.3. In vitro biocompatibility study

3.3.1. ARPE-19 and MIO-M1 cell proliferation in contact with the nanofibers (nuclear count)

The proliferation of ARPE-19 and MIO-M1 cells in direct contact with the PCL nanofibers, DX PCL nanofibers and TCPS control, was measured after 1, 2, 5 and 10 days of incubation. The number of ARPE-19 cells in contact with the nanofibers progressively increased compared to the number of these cells in the TCPS control. Statistical analysis revealed that there was no significant difference in RPE cell proliferation in the presence of the nanofibers and control (one-way ANOVA, $p < 0.05$) after all time intervals of *in vitro* culture (Fig. 5A). The number of MIO-M1 cells in contact with the nanofibers increased at the same rate as in the TCPS control (one-way ANOVA, $p < 0.05$) (Fig. 5B).

3.3.2. Cytotoxicity of PCL nanofibers

Cytotoxicity of PCL nanofibers, DX PCL nanofibers and TCPS control against ARPE-19 and MIO-M1 cells was measured after 1, 2, 5 and 10 days of incubation in direct contact with the nanofibers. Accordingly, the polymeric nanofiber, its degradation products and the released DX showed non-toxicity against these ocular cells, since the viability of RPE and MIO-M1 cells was almost 100% in all time intervals, comparable to the viability of cells in the control medium. The statistical analysis revealed that there was no significant difference in ARPE-19 and MIO-M1 cell viability in the presence of the elements of the drug delivery systems versus the control condition (one-way ANOVA, $p < 0.05$) at any time during *in vitro* culture (Fig. 6A and B, respectively).

3.3.3. Morphology of ARPE-19 and MIO-M1 cells – immunofluorescence

Short-term cultivation of ARPE-19 cells (10 days) in the presence of DX PCL nanofibers led to the production of a confluent layer of cells (Fig. 7F). Stained F-actin fibers revealed the interconnectivity among these fibers, and consequently among the RPE cells, since the actin filaments were running through the upper part of the cytoplasm of different cells. Stained F-actin fibers also demonstrated the existence of a cobblestone format of select adjacent cells (Fig. 7E). Stained nuclei

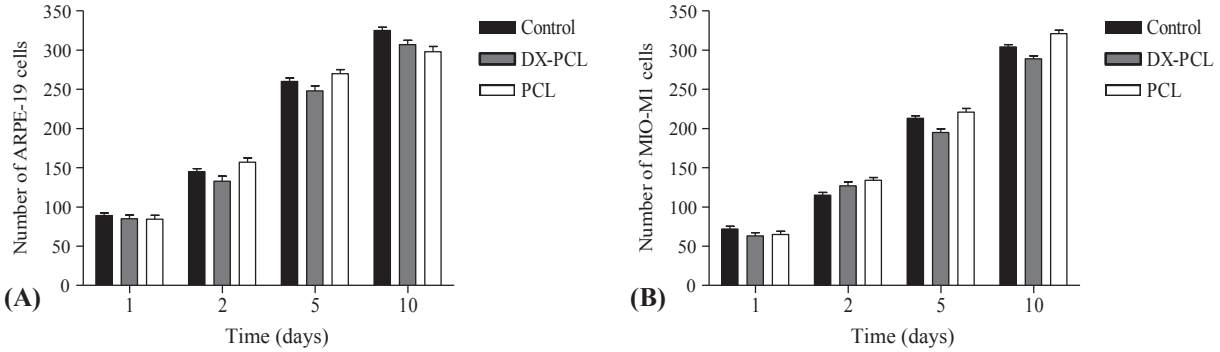

Fig. 5. Proliferation kinetics of ARPE-19 cells (A) and MIO-M1 cells (B) cultured in direct contact with the PCL nanofibers, DX PCL nanofibers and TCPS control for 1, 2, 5 and 10 days of incubation. Data were expressed as the mean number of nuclei ± standard deviation for each time point (n = 10 per group, per day) ($p < 0.05$).

demonstrated that they were homogeneously distributed as a monolayer and centrally located without overlap. The large number of nuclei represented the high density of RPE cells. In addition, stained nuclei also revealed the presence of cells in the process of division (Fig. 7D). Analyses of the morphology of ARPE-19 cells in the control medium revealed similar results to those obtained for cultures grown in contact with the PCL nanofibers incorporated into the DX. After 10 days of incubation, the control RPE cells reached confluence (Fig. 7C), the actin filaments formed a complex network (Fig. 7B), the nuclei did not overlap, and some of them were performing nuclear division (Fig. 7A).

Short-term cultivation of the MIO-M1 cells (10 days) in contact with the DX PCL nanofibers led to the formation of a monolayer of the retinal glial cells (Fig. 7L). They expressed the microfilament actin, which revealed the presence of elongated and radially oriented cells (Fig. 7K). Nuclei were ellipsoid and highly centralized (Fig. 7J). The morphology of MIO-M1 cells grown on the glass coverslips demonstrated the same typical features of Muller cells in the presence of drug delivery systems (Fig. 7G, H and I). Muller cells in contact with the drug delivery systems for 10 days demonstrated their ability to express the glial fibrillary acidic protein (GFAP) (Fig. 8F) similarly to the control cells (Fig. 8C). GFAP is a universal MIO-M1 cell marker present in the glial cytoplasm that is often used to identify this cell population [26].

3.4. In vivo biocompatibility study

3.4.1. In vivo retinal imaging using OCT

Fig. 9 depicts the *in vivo* SD-OCT scans of tissues of the posterior segment of rat eyes, which did not receive the polymeric nanofibers (control) (Fig. 9A), or rat eyes that received the DX PCL nanofibers (Fig. 9B) after 10 days of implantation in the vitreous cavity of rat eyes. Retinal layers and choroid were not affected by either the presence of PCL nanofibers and their degradation products or by the released drug, once the architecture of these tissues was preserved. SD-OCT *in vivo* retinal imaging did not show any abnormalities. The choroidal and retinal thickness did not differ between the animals of the control group and the animals receiving the DX PLC nanofibers (Student's *t*-test, $p < 0.05$) (Fig. 9C). The qualitative analysis of SD-OCT images corroborated the quantitative evaluation of the thickness of specific ocular tissues, and these results confirmed the short-term biocompatibility of nanometric drug delivery systems.

3.4.2. Morphology

The morphologies of tissues of the posterior segment of the rat eyes of the control group (Fig. 10A) and animals receiving DX PCL nanofibers (Fig. 10B) were evaluated 10 days after implantation in the vitreous cavity. The architecture of the ocular tissues of both groups was similar, and it was completely preserved: (1) neuroretina and RPE layer were tightly attached; (2) photoreceptors were not damaged; and (3) choroid and sclera were intact. Furthermore, signs of an inflammatory response were not detected due to the absence of an inflammatory infiltrate in the posterior tissues of the eye and in the vitreous cavity, as well as the nonexistence of a hemorrhagic process and angiogenesis. Therefore, the histological examination demonstrated that the PCL nanofibers, their degradation products, and the DX released from the systems were not toxic to the ocular tissues of the posterior eye. These drug delivery systems did not induce any damage to the ocular tissues of the anterior segment of the eye and were well tolerated (histological sections not shown). Finally, the choroid thickness was measured, and there was no significant difference between animals of the control group and animals receiving the DX PCL nanofibers (Student's *t*-test, $p < 0.05$). The retinal layer thickness in the middle pole was also measured, and there was no significant difference between animals of the control group and animals receiving DX PCL nanofibers (Student's *t*-test, $p < 0.05$) (Fig. 10C).

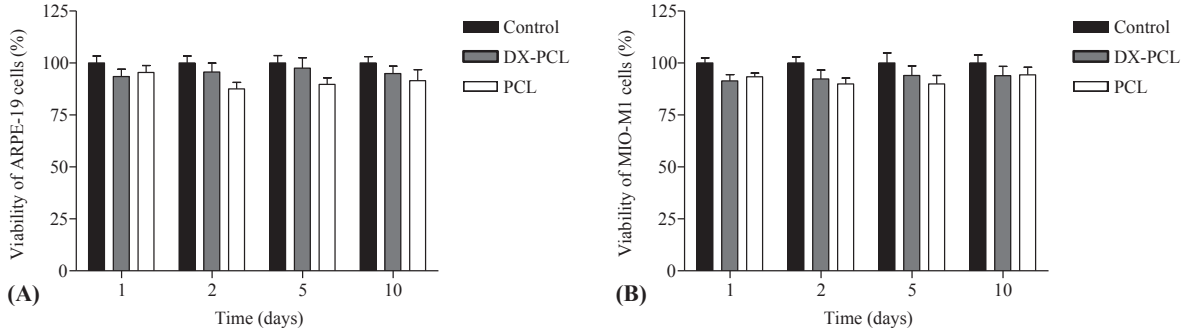

Fig. 6. Viability of ARPE-19 cells (A) and MIO-M1 cells (B) cultured in the presence of PCL nanofibers, DX PCL nanofibers and TCPS control after 1, 2, 5 and 10 days of incubation (n = 10 for each group, per day) ($p < 0.05$). The viability of these ocular cells in contact with blank nanofibers and DX PCL nanofibers was determined relative to the control, which was fixed at 100%.

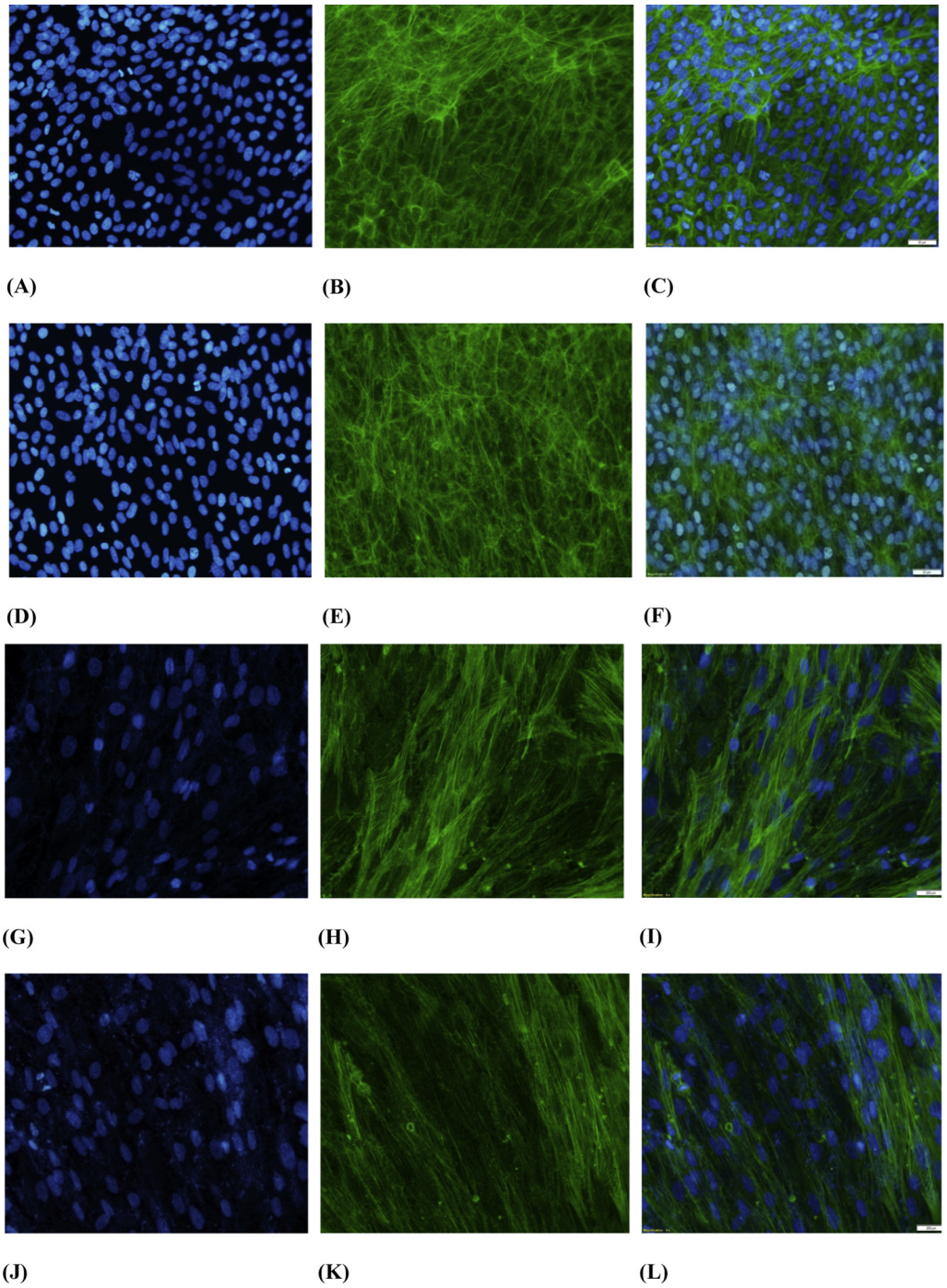

Fig. 7. Photomicrographs of ARPE-19 cells in the control medium (A, B, C), and in direct contact with DX PCL nanofibers (D, E, F), during 10 days of incubation. Nuclei were stained with DAPI (blue) (A and D), and F-actin filaments were stained with Phalloidin FITC (green) (B and E). The merge of nuclei and F-actin filaments was represented in the micrographs C and F (×20). Photomicrographs of MIO-M1 cells onthe glass coverslips (G, H, I) and in the presence of DX PCL nanofibers (J, K, L) are shown after 10 days of incubation. Nuclei (blue) (G and J) and F-actin filaments (green) (H and K) were stained with DAPI and Phalloidin FITC, respectively. The merge of nuclei and F-actin filaments was represented in the micrographs I and L (×40). (For interpretation of the references to colour in this figure legend, the reader is referred to the web version of this article.)

3.4.3. Immunohistochemistry on cryosections

Fig. 11 shows the cone photoreceptors present in the retina of rat eyes of the control group (Fig. 11A) and the DX PCL nanofiber group (Fig. 11D). The outer segment and synaptic bodies of cone photoreceptors were entirely stained. They appeared as a highly organized layer. Fig. 11 also demonstrates the outer segments of rod photoreceptors present in the retina of rat eyes of both groups (Fig. 11H and I). The rod photoreceptor layer was undamaged. The preservation of photoreceptor layers suggested the absence of retinal degeneration.

4. Discussion

Post-operative inflammation following vitreoretinal surgery, particularly when indicated for retinal detachment, contributes to proliferative vitreoretinopathy, a severe complication that leads to recurrence of detachment [27]. It also contributes to macular edema that reduces visual recovery. Proliferative vitreoretinopathy is a complex process involving ischemic tissue damage, inflammation, and proliferation of several types of cells, as well as the production of local factors [28]. Initiation of the apoptotic response may be mediated in part by the release of cytokines from the stressed and damaged tissues [27,28]. At the same time, and because of the breakdown of blood retinal barriers, microglia and macrophages migrate into the subretinal space, and into the vitreous cavity, where they release inflammatory mediators, creating a pro-inflammatory and angiogenic environment. There is no consensus regarding the optimal post-operative anti-inflammatory treatment after vitreoretinal surgeries, but most ophthalmologists agree that retinal detachment and combined anterior and

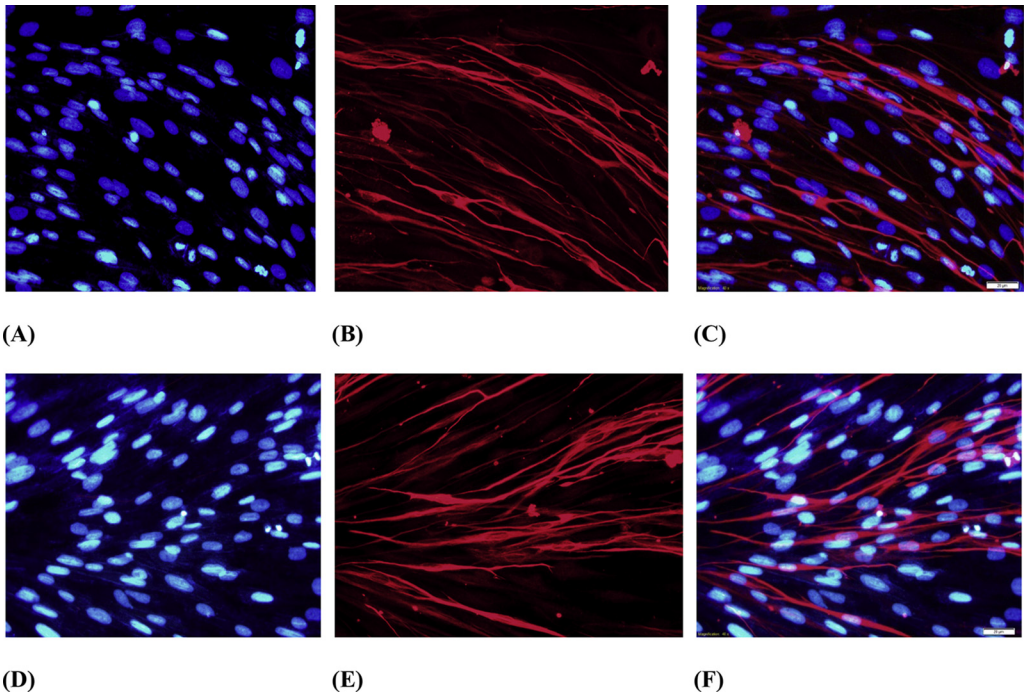

Fig. 8. Photomicrographs of MIO-M1 cells onthe glass coverslips (A, B, C) and in the presence of the DX PCL nanofibers (D, E, F) after 10 days of incubation. Nuclei (blue) (A and D) and GFAP (red) (B and E) were stained with DAPI and GFAP marker, respectively. The merge of nuclei and GFAP isrepresented in the micrographs C and F (×40). (For interpretation of the references to colour in this figure legend, the reader is referred to the web version of this article.)

posterior segments surgeries are most prone to induce inflammation and would prescribe more intensive preventive treatment in such cases [29]. Intravitreal DX injections can be proposed but has a short efficacy because DX half-life in the vitreous ranges from 2 to 6 h [29]. A drug delivery system that could be left into the vitreous and release DX for 1 to 2 weeks would ensure an appropriate post-operative anti-inflammatory therapy, suppressing the need for multiple daily instillation of drops, which penetration in the posterior segment of the eye remains uncertain. The electrospun nanofibers composed of PCL and DX could be appropriate for this indication. Having demonstrated the excellent tolerance of empty PCL nanofibers on retinal cells *in vitro* as well as *in vivo* after intravitreous injection in the rat's eye [15], we evaluated herein their potential to release dexamethasone for several days to weeks to prevent the inflammation after ocular surgeries. Since local high dexamethasone dose can elicit retinal cells toxicity [17], we also have evaluated the tolerance of PCL nanofibers loaded with

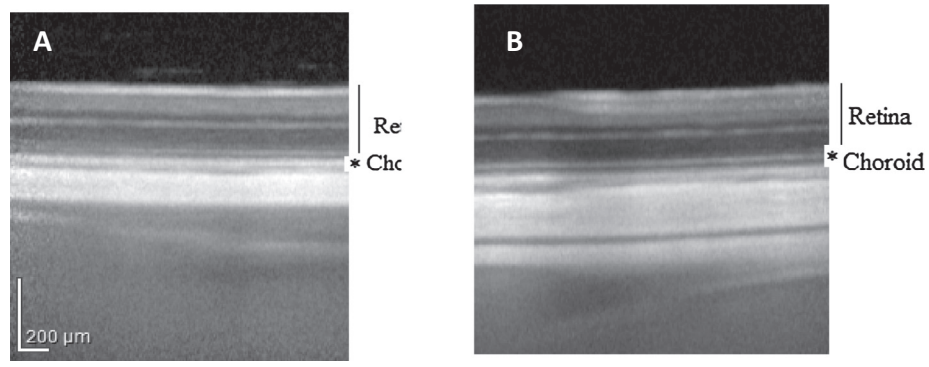

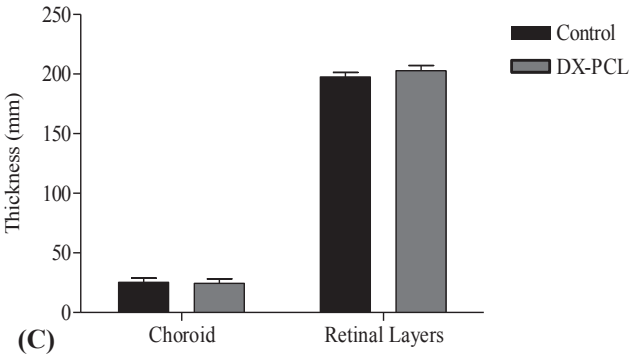

Fig. 9. SD-OCT images of choroid and retinal layers of control group rat eyes (A), and those of animals receiving DX PCL nanofibers (B), after 10 days of implantation. Retinal layers and choroid were highlighted. Thickness of choroid and retinal layers of the rat eyes of the control group and animals in contact with DX PCL nanofibers (C) (n = 6 per group) ($p < 0.05$). Scale bar – 200 µm.

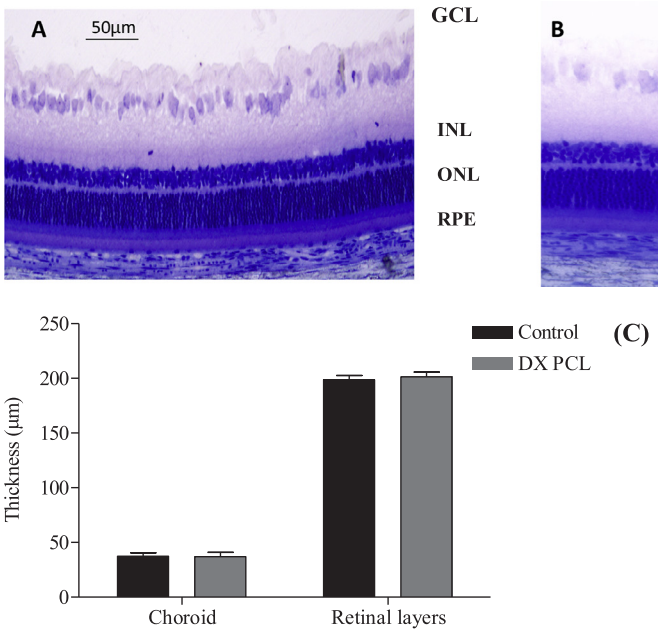

Fig. 10. Histological sections of retinal layers and choroid obtained 10 days after implantation of DX PCL nanofibers in the vitreous cavity of rat eye (A) and control group (B) (toluidine blue) (×20). Thickness of choroid and retinal layers of the rat eyes of the control group and animals in contact with DX PCL nanofibers (C) (n = 6 per group) ($p < 0.05$). GCL: Ganglion Cell Layer, INL: Inner Nuclear Layer, ONL: Outer Nuclear Layer, RPE: retinal pigment epithelium. (For interpretation of the references to colour in this figure legend, the reader is referred to the web version of this article.)

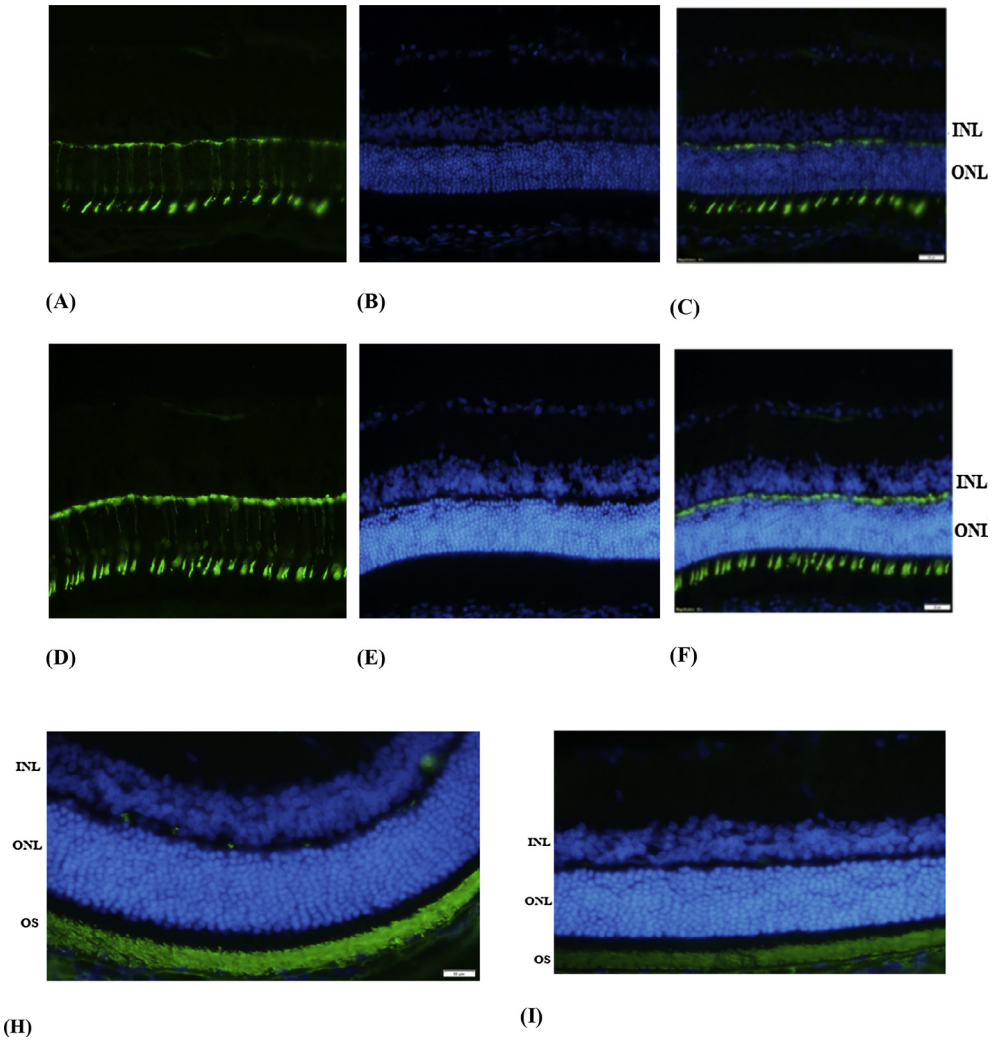

Fig. 11. Cone arrestin stained the entire cone photoreceptors, including outer segments and synaptic bodies in the rat eyes of the control group (A) and in the animals in contact with the DX PCL nanofibers (D) (green). Nuclei of outer nuclear layer (ONL) and inner nuclear layer (INL) were stained with DAPI (blue) (B and E). The merge of cone photoreceptors and nuclei was represented in the micrographs C and F (×40). Rhodopsin stained the outer segments (OS) of rod photoreceptors in the rat eyes of the control group (H) and in eyes of animals in contact with the DX PCL nanofibers (I) (green) (×60). (For interpretation of the references to colour in this figure legend, the reader is referred to the web version of this article.)

dexamethasone on retinal cells viability. The nanofibers were prepared by dissolving PCL and DX in a mixture of organic solvents (1:1 formic and acetic acids). Only acetic acid did not enable the formation of PCL nanofibers, due to its low dielectric constant (Ɛ = 6.2) [31]. Consequently, formic acid, which has a high dielectric constant (Ɛ = 58) [30], was added into the composition of the mixture of solvents, resulting in electrospinnability of the polymer and drug solution and, subsequently, the formation of thinner PCL DX nanofibers with fewer beads. It was described that the high electrical conductivity of the solution generally leads to the formation of nanofibers with lower bead content [32]. These monolithic hydrophobic nanofibers exhibited random orientation with no phase separation as drug crystals were not observed in the surface. In addition, the DX homogeneously distributed into the polymeric chains (as detected by the content uniformity) did not modify the morphology of nanometric fibers, which presented a cylindrical shape and porosity.

PCL nanofibers provided the controlled release of DX over a 12 days period with an initial burst within the first 2 days. This initial release could result from the rapid diffusion of the drug located at the nanofiber surfaces and/or to the initial degradation of the PCL. Indeed, the superficial deposition of DX on the nanofibers occurred during the evaporation of the solvent mixture in the electrospinning technique and the FTIR results confirmed the weak chemical interactions between drug and the PCL. On the other hand, the initial release could be due also to the 25% of PCL mass loss during this time period. Afterwards, PCL nanofibers modulated the release of DX, driven by desorption of the drug and degradation of the polymer. It was suggested that the nanopores filled with water could induce desorption of the drug from the interior of nanofibers inducing the diffusion of DX in water from the pore [23]. The uptake of water and the desorption mechanism of the drug occurred due to the presence of porous structure and the large surface-area-to-volume ratio. These elements associated with the existence of ultrafine fibers also contributed to the rapid degradation of PCL and, consequently, the lixiviation of DX from the systems. The degradation of PCL nanofibers could be experimentally demonstrated by their progressive mass loss after the period of 12 days of immersion in PBS, suggesting that no empty polymer would remain in the eye after the drug has been released. This type of release profile is well adapted to the postoperative period, when inflammation is at its maximal intensity after the procedure and then slowly decrease in the following days.

Metronidazole and ciprofloxacin hydrochloride loaded both individually or in combination into hydrophobic poly(ε-caprolactone) matrix using electrospinning showed a similar initial burst [24]. According to Zupancič et al., the PCL macromolecules could be hydrolyzed in the presence of organic acids [24] (as detected in the FTIR analyses), resulting in a mixture of PCL macromolecules of different chain lengths. The hydrolysis of ester bonds in PCL chains increased the amount of carboxyl and hydroxyl groups in the nanofibers. The –COOH group was ionized in the PBS solution and increased the hydrophilicity of the polymer when associated with –OH. Water uptake into the nanometric fibers was completely favorable when the PCL macromolecule was more hydrophilic, inducing not only the degradation of the polymer but also the dissolution of DX and, consequently, its release into the medium. However, in spite of the PCL degradation, the drug was released in a sustainable fashion; this effect was probably due to the existence of PCL with different chain lengths, which were gradually hydrolyzed, contributing to an enduring and progressive drug release.

Despite PCL being considered as a biodegradable and biocompatible polymer that does not induce an inflammatory response in a biological environment, the PCL was solubilized in acidic solvents to prepare the nanometric fibers. The possibility of the inclusion of acidic solvent residues into the mats could threaten toxicity to the delicate ocular tissues and consequently disrupt the neurosensorial retina and other ocular structures, resulting in the failure of the ophthalmic application of these drug delivery systems. Moreover, the degradation profile of PCL nanofibers is different from the same polymer at the macroscale. The PCL is characterized by a very low hydrolysis rate, which can extend over a period of more than 1 year [33]. In contrast, PCL nanofibers showed an extremely rapid degradation profile, and almost 100% was degraded in 12 days in PBS due to the ultrafine structure, high porosity, and high surface-area-to-volume ratio of the polymer. The faster rate of degradation of PCL nanofibers could result in the accumulation of acidic by-products, contributing to the acidification of the ocular microenvironment. Testing the ocular tolerance of this new drug delivery system was thus a prerequisite to any further development.

The *in vitro* biocompatibility study using ARPE-19 and MIO-M1 cells revealed that neither the acidic PCL degradation products, nor the accumulated dexamethasone acetate released from PCL nanofibers, induced cytotoxicity (as detected by MTT test); consequently, these ocular cells were capable of proliferating with a typical morphology. According to Verdugo-Gazdik et al., active processes can provoke alterations in the structure of actin filaments, and this parameter can be used as a potential marker of drug-induced retinal toxicity [33]. Because the actin microfilaments from ARPE-19 cells provided for the formation of polygonal arrays, adherens junctions between cells, and the generation of a complex fiber network that is responsible for the stabilization of the microvilli protrusions and internalization phagocytosis of outer segments [34,35], it was suggested that this cellular biomarker was not affected by DX PCL nanofibers and the polymeric by products. According to Martinez-De Luna et al., Muller cell gliosis, a response to injury and disease in the retina, induces the upregulation of the expression of GFAP and, consequently, the modification of cellular morphology [36]. Therefore, GFAP is a universal marker of this cell population and was not damaged by DX PCL nanofibers or the polymeric degradation products. Finally, considering the fact that retinal pigment epithelial (RPE) cells and glial cells are the retinal cell populations implicated in the evolution of proliferative vitreoretinopathy and capable to produce cytokines [37], these cells and their phenotypic biomarkers must be selected to investigate the toxicity of drug delivery systems intended to treat this ocular disease.

After demonstrating the *in vitro* biocompatibility and short-term *in vivo* biocompatibility of DX PCL nanofibers, they were further assessed by implantation into rat vitreous cavities. SD-OCT produced high-resolution images that revealed the integrity of neuroretina and choroid in direct contact with nanofibers and their components. These ocular tissues are extremely sensitive to toxic agents [36]. SD-OCT results also allowed for measuring the thickness of retinas and choroids, without eye enucleation, demonstrating that this parameter was unchanged in the animals receiving DX PCL nanofibers when compared to those of the control group. The modification of retinal and choroidal thickness is a common sign of ocular toxicity [37].

Acidic PCL degradation products are water soluble and are excreted *via* the trabecular meshwork outflow to the venous circulation [38] contributing to reduced/inhibited retinal damage. In addition, cone and rod photoreceptors were also morphologically preserved after exposure to DX PCL nanofibers and polymeric by-products. The integrity of rod and cone photoreceptors suggested that the animals receiving the nanofibers remained light-sensitive and capable of detecting a photon in the dark, as well as able to utilize daylight vision to detect a moving object [38].

5. Conclusion

In this study, electrospun DX PCL nanofibers were designed for intravitreal delivery of corticosteroid for a controlled duration after vitreoretinal surgery. These nanofibers were composed of interconnected fibers arranged in a complex network allowing degradation and DX release for 12 days. DX PCL nanofibers and the byproducts of the polymer exhibited excellent cellular biocompatibility on ARPE-19 and MIO-M1 cells *in vitro* as well as *in vivo* after vitreous implantation in the rat eye. Before any clinical translation can be envisaged, further studies

are required to test adequate sterilization methods, accepted by regulatory agencies, as well as upscaling possibilities.

Declaration of Competing Interest

The authors declare no conflict of interest.

Acknowledgements

The authors thank the CNPq/MCT (Brazil), Fapemig (Brazil, Grant APQ 01522-16), and CAPES (Bolsistas da CAPES-Brasília/Brazil) for the financial support.We think Astrid Limb for providing the human glial cell line MIO-M1.

References

[1] X. Hu, S. Liu, G. Zhou, Y. Huang, Z. Xiea, X. Jing, Electrospinning of polymeric nanofibers for drug delivery applications, J. Control. Release 185 (2014) 12–21.
[2] G. Taylor, Electrically driven jets, Proc. R. Soc. Lond. A. 313 (1969) 453–475.
[3] J. Zeng, X. Xu, X. Chen, Q. Liang, X. Bian, L. Yang, X. Jing, Biodegradable electrospun fibers for drug delivery, J. Control. Release 92 (2003) 227–231.
[4] W. Zhao, W. Liu, J. Li, X. Lin, Y. Wang, Preparation of animal polysaccharides nanofibers by electrospinning and their potential biomedical applications, J. Biomed. Mater. Res. A. 103 (2) (2015) 807–818.
[5] A. Touseef, M.S. Hassan, H.V. Ba, K. Myung-Seob, L. Hak-Kyo, I.H. Hwang, Electrospun Fe_3O_4/TiO_2 hybrid nanofibers and their in vitro biocompatibility: prospective matrix for satellite cell adhesion and cultivation, Mat. Sci. Eng. C. 33 (2013) 707–713.
[6] L. Tian, M.P. Prabhakaran, S. Ramakrishna, Strategies for regeneration of components of nervous system: scaffolds, cells and biomolecules, Regen. Biomater. 2 (1) (2015) 31–45.
[7] P. Xiang, K.-C. Wu, Y. Zhu, L. Xiang, C. Li, D.-L.C.F. Chen, G. Xuc, A. Wang, M. Li, Z.-B. Jin, A novel Bruch's membrane-mimetic electrospun substrate scaffold for human retinal pigment epithelium cells, Biomaterials 35 (2014) 9777–9788.
[8] Z. Liu, N. Yu, F.G. Holz, F. Yang, B.V. Stanzel, Enhancement of retinal pigment epithelial culture characteristics and subretinal space tolerance of scaffolds with 200 nm fiber topography, Biomaterials 35 (9) (2014) 2837–2850.
[9] Š. Zupančič, S. Sinha-Ray, S. Sinha-Ray, J. Kristl, A.L. Yarin, Long-term sustained ciprofloxacin release from PMMA and hydrophilic polymer blended nanofibers, Mol. Pharm. 4 (13(1)) (2016) 295–305.
[10] P. Mehta, A.A. Al-Kinani, M.S. Arshad, M.W. Chang, R.G. Alany, Z. Ahmad, Development and characterisation of electrospun timolol maleate-loaded polymeric contact lens coatings containing various permeation enhancers, Int. J. Pharm. 30 (532) (2017) 408–420.
[11] X. Li, Y. Wang, C. Yang, S. Shi, L. Jin, Z. Luo, J. Yu, Z. Zhang, Z. Yang, H. Chen, Supramolecular nanofibers of triamcinolone acetonide for uveitis therapy, Nanoscale 6 (23) (2014) 14488–14494, https://doi.org/10.1039/C4NR04761C.
[12] S. Mirzaeei, K. Berenjian, R. Khazaei, Preparation of the potential ocular inserts by electrospinning method to achieve the prolong release profile of triamcinolone acetonide, Adv. Pharm. Bull. 8 (1) (2018) 21–27.
[13] G. Uzunalli, Z. Soran, T.S. Erkal, Y.S. Dagdas, E. Dinc, A.M. Hondur, K. Bilgihan, B. Aydin, M.O. Guler, A.B. Tekinay, Bioactive self-assembled peptide nanofibers for corneal stroma regeneration, Acta. Biomater. 10 (3) (2014) 1156–1166.
[14] S.O.L. de Souza, M.C.A. Guerra, L.G.D. Heneine, C.R. de Oliveira, A.D.S. Cunha Junior, S.L. Fialho, R.L. Oréfice, Biodegradable core-shell electrospun nanofibers containing bevacizumab to treat age-related macular degeneration, J. Mater. Sci. Mater. Med. 3;29(11) (2018) 173–184.
[15] G.R. Da Silva, T.H. Lima, R.L. Oréfice, G.M. Fernandes-Cunha, A. Silva-Cunha, M. Zhao, F. Behar-Cohen, In vitro and in vivo ocular biocompatibility of electrospun poly(ε-caprolactone) nanofibers, Eur. J. Pharm. Sci. 20 (73) (2015) 9–19.
[16] S.A.L. Moura, L.D. Lima, S.P. Andrade, A. Da Silva-Cunha, R.L. Órefice, E. Ayres, G.R. Da Silva, Local drug delivery system: inhibition of inflammatory angiogenesis in a murine sponge model by dexamethasone-loaded polyurethane implants, J. Pharm. Sci. 100 (7) (2011) 2886–2895.
[17] F. Valamanesh, A. Torriglia, M. Savoldelli, C. Gandolphe, J.C. Jeanny, D. BenEzra, F. Behar-Cohen, Glucocorticoids induce retinal toxicity through mechanisms mainly associated with paraptosis, Mol Vis. 19 (13) (2007) 1746–1757 Sep.
[18] O. Tomkins-Netzer, S.R. Taylor, A. Bar, A. Lula, S. Yaganti, L. Talat, S. Lightman, Treatment with repeat dexamethasone implants results in long-term disease control in eyes with noninfectious uveitis, Ophthalmology 121 (8) (2014) 1649–1654.
[19] The United States Pharmacopeial Convention, 34th ed.; Rockville: MD, 2011.
[20] G.A. Limb, T.E. Salt, P.M. Munro, S.E. Moss, P.T. Khaw, In vitro characterization of a spontaneously immortalized human Muller cell line (MIO-M1), Invest. Ophthalmol. Vis. Sci. 43 (2012) 864–869.
[21] M.D. Fischer, G. Huber, S.C. Beck, N. Tanimoto, R. Muehlfriedel, E. Fahl, C. Grimm, A. Wenzel, C.E. Remé, S.A. Van de Pavert, J. Wijnholds, M. Pacal, R. Bremner, M.W. Seeliger, Non-invasive, in vivo assessment of mouse retinal structure using optical coherence tomography, PLoS ONE 4 (10) (2009) 7507–7514.
[22] M.M. Coleman, J. Zarian, Fourier transform InfraRed studies of polymer blends. II. Poly(ϵ-caprolactone)–poly(vinyl chloride) system, J. Polym. Sci. B. 17 (1979) 837–850.
[23] T. Elzein, M. Nasser-Eddine, C. Delaite, S. Bistac, P. Dumas, FTIR study of polycaprolactone chain organization at interfaces, J. Coll. Interf. Sci. 273 (2) (2004) 381–387 15.
[24] S. Zupančič, L. Preem, M. Putrins, T. Tenson, P. Kocbek, K. Kogermann, Impact of PCL nanofiber mat structural properties on hydrophilic drug release and antibacterial activity on periodontal pathogens, Eur. J. Pharm. Sci. 15 (122) (2018) 347–358.
[25] G.R. Silva, A. Silva-Cunha, F. Behar-Cohen, E. Ayres, R.L. Oréfice, Biodegradable polyurethane nanocomposites containing dexamethasone for ocular route, Mater. Sci. Eng. C 31 (2011) 414–422.
[26] L. Shao-Fen, M. Yu-Xiang, L. Bin, S. Wei, T. Shi-Bo, Morphological and immunocytochemical analysis of human retinal glia subtypes in vitro, Int. J. Ophthalmol. 6 (5) (2013) 559–563.
[27] J.C. Pastor, J. Rojas, S. Pastor-Idoate, S. Di Lauro, L. Gonzalez-Buendia, S. Delgado-Tirado, Proliferative vitreoretinopathy: a new concept of disease pathogenesis and practical consequences, Prog. Retin. Eye. Res. 51 (2016) 125–155.
[28] J.G. Garweg, C. Tappeiner, M. Halberstadt, Pathophysiology of proliferative vitreoretinopathy in retinal detachment, Surv. Ophthalmol. 58 (4) (2013) 321–329.
[29] F. Aptel, C. Colin, S. Kaderli, C. Deloche, A.M. Bron, M.W. Stewart, C. Chiquet, OSIRIS group, Management of postoperative inflammation after cataract and complex ocular surgeries: a systematic review and Delphi survey, Br. J. Ophthalmol. 101 (11) (2017) 1–10.
[30] S.S. Lee, P. Hughes, A.D. Ross, M.R. Robinson, Biodegradable implants for sustained drug release in the eye, Pharm. Res. 27 (10) (2010) 2043–2053.
[31] C.J. Luo, E. Stride, M. Edirisinghe, Mapping the influence of solubility and dielectric constant on electrospinning polycaprolactone solutions, Macromolecules 45 (11) (2012) 4669–4680.
[32] T. Potrč, S. Baumgartner, R. Roškar, O. Planinšek, Z. Lavrič, J. Kristl, P. Kocbek, Electrospun polycaprolactone nanofibers as a potential oromucosal delivery system for poorly water-soluble drugs, Eur. J. Pharm. Sci. 30 (75) (2015) 101–113.
[33] A.G.R. Solano, A.F. Pereira, F.C.H. Pinto, L.G.R. Ferreira, L.A.O. Barbosa, S.L. Fialho, P.S.O. Patrício, A. Silva-Cunha, G.R. Silva, G.A. Pianetti, Development and evaluation of sustained-release etoposide-loaded poly(ε-caprolactone) implants, AAPS PharmSciTech. 14 (2) (2013) 890–900.
[34] M.E. Verdugo-Gazdik, D. Simic, A.C. Opsahl, M.W. Tengowski, Investigating cytoskeletal alterations as a potential marker of retinal and lens drug-related toxicity, Assay. Drug. Dev. Technol. 4 (6) (2006) 695–707.
[35] S.K. Fisher, R.H. Steinberg, Origin and organization of pigment epithelial apical projections to cones in cat retina, J. Comp. Neurol. 206 (1982) 131–145.
[36] R.I. Martinez-De Luna, R.Y. Ku, A.M. Aruck, F. Santiago, A.S. Viczian, D.S.S. Mauro, M.E. Zuber, Müller glia reactivity follows retinal injury despite the absence of the glial fibrillary acidic protein gene in Xenopus, Dev. Biol. 426 (2) (2017) 219–235 15.
[37] A. Sadaka, G.P. Giuliari, Proliferative vitreoretinopathy: current and emerging treatments, Clin. Ophthalmol. 6 (2012) 1325–1333.
[38] Y.-S. Hwang, P.R. Chiang, W.H. Hong, C.C. Chiao, I.M. Chu, G.H. Hsiue, C.R. Shen, Study in vivo intraocular biocompatibility of in situ gelation hydrogels: poly(2-ethyl oxazoline) block poly(ε-caprolactone)-block-poly(2-ethyl oxazoline) copolymer, matrigel and pluronic F127, PLoS One 8 (7) (2013) e67495 1.